TTCM-Assisted Distributed Source-Channel Coding for Nakagami-m Fading Channels

Abdulah Jeza Aljohani, Soon Xin Ng, and Lajos Hanzo

University of Southampton
Communications, Signal Processing and Control Research Group
Southampton, SO17 1BJ, U.K.
E-Mail: {ajra1c09,sxn,lh}@ecs.soton.ac.uk

***Abstract*— Asymmetric Distributed Source-Channel coding (DSC) is considered, where a pair of correlated sources are transmitting to a central node. The distributed scheme is based on Turbo Trellis Coded Modulation (TTCM), where the first source will be channel encoded and then compressed before it is sent over Nakagami-m fading channels. The second source signal, however, is assumed to be available flawlessly at the destination for exploitation as side information for improving the decoding performance of the first source. A wide range of fading scenarios were considered, where reliable communications approaching the Slepian-Wolf Shannon (SW/S) limit were exhibited. Finally, the scheme is capable of adapting to the time-variant short-term correlation between the two sources.**

***Index Terms*— DSC, Slepian-Wolf Coding, Joint Source Channel Coding, TTCM, Nakagami.**

I. Introduction

Driven by its diverse range of applications, such as distributed sensor networks [1], efficient video transmission [2] and stereo solar satellites imagery compression [3], Distributed Source Coding (DSC) has recently attracted substantial research interests both in academia and industry. DSC refers to the problem of separate compression and joint decoding (or decompression) of several physically separated, but correlated sources [1]. Applying DSC techniques, such as Slepian-Wolf (SW) coding [4] or Wyner-Ziv (WZ) coding, has facilitated efficient and low-cost signal processing in sensor networks, where the complexity has been moved from the battery-limited nodes to the central Base Station (BS) [1].

The SW coding theorem [4] characterises the region of achievable rates R_1 and R_2 in the case of lossless compression of two correlated sources $\mathbf{b}_1$ and $\mathbf{b}_2$ communicating with a joint decoder. The region, as it will be detailed in Fig. 5 during our further discourse, can be drawn as a polygon defined by two corners, where the SW bounds is obtained by: $R_1 \geq H(b_1|b_2)$, $R_2 \geq H(b_2|b_1)$ and $R_1 + R_2 \geq H(b_1, b_2)$, where $H(b_1|b_2)$ and $H(b_1, b_2)$ denote the conditional and joint entropies, respectively. Surprisingly, regardless, whether joint processing takes place or not i.e. regardless of whether joint encoding was invoked, the bounds in both scenarios are identical.

The close connection between the SW coding and channel coding[1] has facilitated the employment of practical channel coding techniques for approaching the SW limit. Many practical channel codes were proposed for SW coding. For example, turbo codes (TC) were proposed for SW coding in [6], and low-density parity-check (LDPC) codes were considered in [7], [8], whereas polar and raptor codes were employed in [2], [9], respectively. However, finding the best code for approaching the Slepian-Wolf Shannon (SW/S) limit was not considered in [2], [6], [7], [9].

Later, many schemes were proposed for more realistic scenarios aiming for approaching the SW/S limit. In [10] for example a "super" TC was proposed for Additive White Gaussian Noise (AWGN) channels. Then, a low-density generator-matrix (LDGM) code has been proposed in [11], when communicating over Rayleigh fading channels. However, the scheme in [10] suffers from a high error floor, when considering a Rayleigh fading channel, while in [11] a high error floor persists, when the correlation value is low. Recently, in [12] an iterative joint-turbo equaliser and decoder scheme was proposed for transmission over a multi-path fading channel. In [12] near-SW/S performance was achieved, albeit at the cost of a high joint decoding complexity, requiring as many as 350 decoding iterations.

Against this background, in this treatise we further extend the adaptive DSC-based turbo trellis coded modulation (TTCM) (A-DSTTCM) scheme of [13] into a wide range of realistic Nakagami-m fading scenarios. The proposed scheme shows a capability of achieving a near-SW/S performance without exhibiting an error floor for a wide range of both Nakagami-m *fading parameters* as well as for diverse source correlation values ρ[2]. The novel adaptive scheme of [13] is also invoked for maintaining a given target bit error ratio (BER), while accommodating both the near-instantaneous fluctuation of the channel quality, which may be associated with sensor movements, as well as the short-term correlation variation between the sources, which may also be caused by mobility. Furthermore, we derive the discrete-input continuous-output memoryless channel (DCMC) capacity formula for Nakagami-m channels, in order to specify the SW/S limit of all scenarios considered.

This paper is organised as follows. Our system model is described in Section II, while the corresponding rate region is designed in Section II. Our performance results are discussed in Section IV. Finally, our conclusion are offered in Section V.

II. System Model

We consider the asymmetric DSC system of Fig. 1 [6], where the source-bit frame $\mathbf{b}_1$ is compressed before its transmission. However, the correlated source signal $\mathbf{b}_2$ is assumed to be flawlessly available at the decoder, but not at the source $\mathbf{b}_1$. To elaborate a little further, the sequence $\mathbf{b}_2$, which is typically defined as 'side info' [1], [6] is transmitted at the rate of $R_2 = H(b_2)$, where it can also be interpreted as another desired source signal, which was perfectly recovered[3]. Then the correlated sequence $\mathbf{b}_1$ will be compressed for the sake of

The financial support of Saudi Ministry of Higher Education and that of the European Union's Seventh Framework Programme (FP7/2007-2013) under the auspices of the CONCERTO project (grant agreement no 288502) as well as of the RC-UK under the India-UK Advanced technology Centre and of the European Research Council Advanced Fellow Grant and of the Royal Society's Wolfson Research Merit Award is gratefully acknowledged.

[1]Since the correlation between the sources may be interpreted as the ameliorating effect of a "virtual" channel, a good channel code having for example a maximum minimum Hamming distance will be a good SW code [5].

[2]ρ signifies the correlation between the sources and can be estimated as: $\rho = 1 - 2p_e$, where p_e is the crossover probability.

[3]Note, symmetric DSC SW coding [10]–[12], where the side information sequence has to be transmitted through an independent Rayleigh-fading channel, is not considered in this paper due to space-limitations.

978-1-4799-4449-1/14/$31.00 ©2014 Crown

approaching the Slepian-Wolf bound to a rate of $R_1 = H(b_1|b_2)$ in order to achieve the overall rate of $H(b_1, b_2)$. Note that, we have $\mathbf{b}_1 = \{b_1^1, b_1^2, \cdots, b_1^i, \cdots, b_1^N\}$ and $\mathbf{b}_2 = \{b_2^1, b_2^2, \cdots, b_2^i, \cdots, b_2^N\}$, where N is the length of each source sequence.

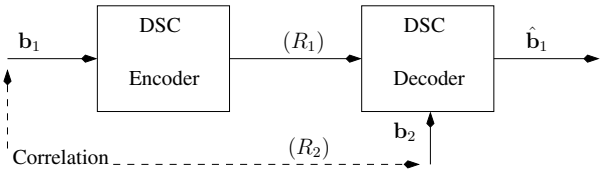

Fig. 1: Schematic diagram of the asymmetric DSC.

Typically, the statistical dependence between the two source sequences is modelled by using a "virtual" binary symmetric channel (BSC) with a crossover probability of p_e. Explicitly, $\mathbf{b}_1$ might be considered as a sequences which was contaminated using a bit-flipping error model with a probability of p_e.The random variables of b_1^i and b_2^i are drawn from the significantly long bit sequences $\mathbf{b}_1$ and $\mathbf{b}_2$. Hence, both the variables b_1^i and b_2^i can be considered as i.i.d. for the bit index i. Thus, both sources emit equiprobable bits [12], consequently, the entropy of each source is unity, giving a conditional entropy of:

$$H(p_e) = H(b_1|b_2) = \lim_{N\to\infty} \frac{i}{1} H\left[\left((b_1^1, \cdots, b_1^i, \cdots b_1^N)|(b_2^1, \cdots, b_2^i, \cdots b_2^N)\right)\right], \quad (1)$$

where $H(p_e) = p_e \log_2\left(\frac{1}{p_e}\right) + (1-p_e)\log_2\left(\frac{1}{1-p_e}\right)$ is the entropy of the binary random variable and e is used for parametrising the side information. Thus, the three SW bound inequalities might be rewritten as [12]:

$$R_1 \geq H(p_e),\ R_2 \geq H(p_e), \quad R_1 + R_2 \geq 1 + H(p_e). \quad (2)$$

In the next three subsections, the design details of our joint source-channel decoding scheme will be discussed, bearing in mind our goal of minimising the signal to noise power ratio (SNR) required for approaching the corresponding SW/S limit.

A. The proposed adaptive distributed source coded modulation

The schematic of the proposed adaptive distributed source coded modulation (A-DSCM) is illustrated in Fig. 2. Similar to [13], $\mathbf{b}_1$ will be fed into a coded modulation encoder. In our simulations we have opted for using TTCM [14] with a code rate of $R_{cm} = \frac{m}{m+1}$. Then, the TTCM-encoded bit-frame $\mathbf{c}_1$ is punctured with a rate of R_p, where the resultant frame $\mathbf{c}_1'$ is mapped to the specific modulated signal $\mathbf{x}_1$, as suggested in Fig. 2. To elaborate further, let us assume that we encode the source $\mathbf{b}_1$ using a rate $R_{cm} = 1/2$ TTCM encoder just before a puncturer of rate $R_p = 2/1$, which punctures the systematic bit out of the two encoded bits. Thus, the overall rate will become $R_1 = R_{cm}\ R_p = 1$. Then, the resultant bits are mapped BPSK symbols, where the modulation mode has been reduced from the original QPSK to BPSK (QPSK/BPSK). Consequently, the effective throughput is estimated using $\eta = R_1 \log_2(2) = 1$ Bit Per Symbol (BPS).

Since our joint decoder is soft-decision-based, we first have to convert the side information sequence $\mathbf{b}_2$ into a LLR sequence using:

$$L(b_2|b_1) = \ln\left[\frac{\Pr(b_2=+1|b_1)}{\Pr(b_2=-1|b_1)}\right] = \ln\left[\frac{(1-p_e)\Pr(b_1=+1) + p_e\Pr(b_1=+1)}{(1-p_e)\Pr(b_1=-1) + p_e\Pr(b_1=-1)}\right]. \quad (3)$$

These LLRs are characterised by the crossover probability p_e, which is assumed to be known at the decoder. The modulated symbol sequence $\mathbf{x}_1$ is transmitted over a Nakagami-m fading channel and the received signal $\mathbf{y}_1$ is given by:

$$\mathbf{y}_1 = \mathbf{h}\mathbf{x}_1 + \mathbf{n}, \quad (4)$$

where $\mathbf{x}_1 = \{x_1^1, x_1^2, \cdots, x_1^i, \cdots, x_1^N\}$ is normalized by the energy constraint $\mathrm{E}\{|x_1|^2\} = 1$, and $\mathbf{n}$ is a zero-mean complex-valued Gaussian noise process having a variance of $N_0/2$ per dimension. In this work, we assume that the channel's fading coefficient $h_i = r_i \exp(j\theta_i)$ is complex and i.i.d, where the phase θ is uniformly distributed and independent from the envelope r. The envelope r follows a wide range of realistic Nakagami-m distribution obeying the probability distribution function (PDF) of [15]:

$$p(r) = \frac{2}{\Gamma(m)}\left(\frac{m}{\Omega_r}\right)\gamma_r^{2m-1}\exp\left(\frac{-mr^2}{\Omega_r}\right), \quad (5)$$

where $\Gamma(\cdot)$ denotes the Gamma function, while $\Omega_r \triangleq \mathrm{E}\{r^2\}$ is the average received power and m represents the fading parameter defined as $m \triangleq \mathrm{E}\{\left(r^2 - \Omega_r\right)^2\}$, where $m \geqslant 0.5$. The Nakagami-m fading channel characterises a wide range propagation scenarios, including both Rayleigh and Ricean fading transmissions. More explicitly, the parameter m characterises the fading depth, where the fading severity will be reduced upon increasing m. For example, when m is equal to its minimum value of $m = 0.5$, Eq.(5) will represent a single-sided Gaussian distribution. By contrast, the Nakagami PDF approaches a Rayleigh fading distribution for $m = 1$, and when we have $m \to \infty$, the channel becomes an AWGN channel. Hence, Nakagami-m can be considered as a generalized distribution that characterising diverse propagation scenarios [15]. Furthermore, the Nakagami-m distribution can be conveniently analysed using both numerical and analytical approaches [15].

The averaged received SNR is given by:

$$\mathrm{SNR}_r = \frac{\mathrm{E}\{|h|^2\}\mathrm{E}\{|x_1|^2\}}{N_0}, \quad (6)$$

where x_1 represents the modulated symbols of the source $\mathbf{b}_1$ after puncturing. Furthermore, we have $\mathrm{E}\{|x_1|^2\} = 1$ and the SNR of $\gamma_r = 10\log_{10}\left(|h|^2/N_0\right)$ [dB] is estimated for each received block. Note that $\mathbf{b}_2$ is related to $\mathbf{b}_1$ according to $b_1^i = b_2^i \oplus e$, as detailed in Section. II. Diverse effective throughputs may be derived by varying R_{cm} and R_p, hence the proposed scheme exhibits a substantial flexibility. In our A-DSCM scheme, the following modes are chosen at the encoder for ensuring that we have BER $< 10^{-5}$:

- No transmission,
- DSCM-QPSK/BPSK,
- DSCM-8PSK/QPSK,
- DSCM-16QAM/8PSK,
- DSCM-32QAM/16QAM.

Thus, the effective throughput of our adaptive system assumes the values of $\eta = \{0, 1, 2, 3, 4\}$ BPS.

At the decoder, the main user's received signal $\mathbf{y}_1$ will be first demapped first for yielding the soft LLR $L(\mathbf{c}_1')$, before it is depunctured, as shown in Fig 2. The novel joint source channel decoder aided TTCM decoder of [13] has been employed. The decoder is constituted by a pair of parallel concatenated trellis coded modulation (TCM) decoders, where both constituent TCM decoders apply the symbol-based MAP algorithm of [16]. Simply, each TCM decoder estimates the A Posteriori Probabilities (APP) using the forward and backward recursion method, while exploiting the side information $L(\mathbf{b}_2')$ [4].

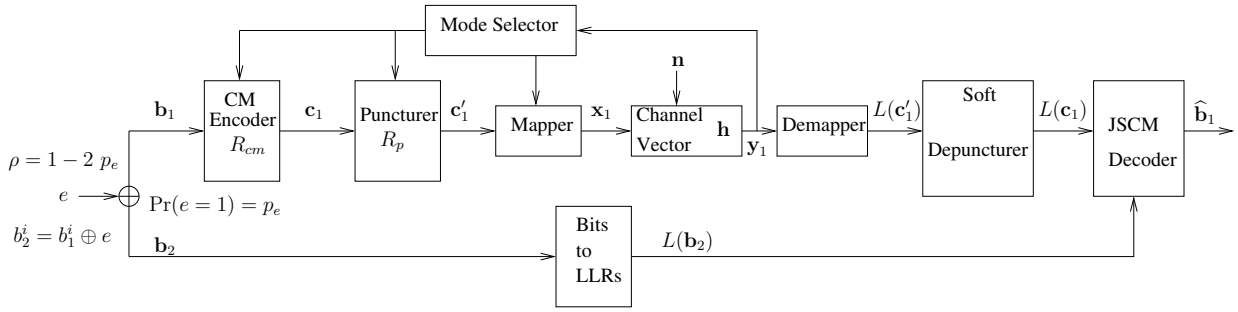

Fig. 2: Schematic of the A-DSCM system communicating over Nakagami-m fading channels. Note that $b_2^i = b_1^i \oplus e$ where $\oplus$ denotes a modulo 2 addition, and $L()$ denotes the Logarithmic-Likelihood Ratios (LLR).

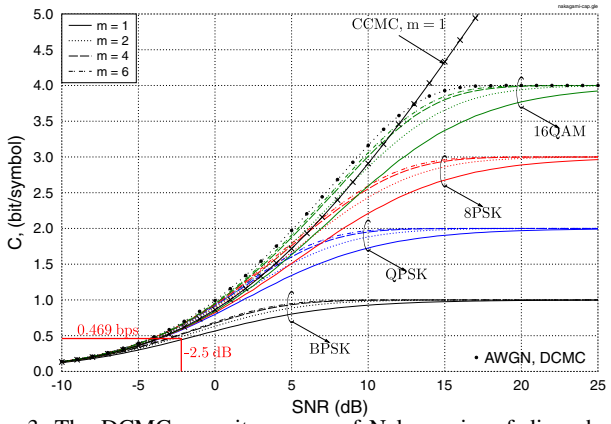

Fig. 3: The DCMC capacity curves of Nakagami-m fading channel for BPSK, QPSK, 8PSK and 16QAM having $m = \{6, 4, 2, 1\}$. Note that CCMC capacity when $m = 1$ as well as AWGN DCMC capacity for 16QAM were included for the sake of comparison, where the curves were computed following the procedure of [17].

III. Rate Region Design and Nakagami-m Capacity

In a noisy environment, the rate region bound defined in Eq. (2) can be rewritten as [10]:

$$H(b_1, b_2) \leq \frac{C_1}{R_1} + \frac{C_2}{R_2} \leq \frac{1}{R_1}\mathrm{E}\left\{\log_2(1+\gamma_1)\right\} + \frac{1}{R_2}\mathrm{E}\left\{\log_2(1+\gamma_2)\right\}, \quad (7)$$

where $C_1 = \mathrm{E}\left\{\log_2(1+\gamma_1)\right\}$ and $C_2 = \mathrm{E}\left\{\log_2(1+\gamma_2)\right\}$ represent the ergodic channel capacities between each of the sources and the destination, while γ_1 and γ_2 are the corresponding received SNRs. However, in our asymmetric design, the side information branch of $\mathbf{b}_2$ is transmitted at $R_2 = H(b_2) = 1$, while our goal is to compress $\mathbf{b}_1$ to the minimum possible rate of $R_1 = H(b_1|b_2)$. Thus, from Eq. (7), the rate region for the main source $\mathbf{b}_1$ branch is given by $R_1\ H(b_1|b_2) \leq C_1$ [18]. Hence, the effective throughput of the scheme can be estimated using $\eta_{SW} = R_1\ H(b_1|b_2)$.

The continuous-input continuous-output memoryless channel (CCMC) capacity of an uncorrelated Nakagami-m fading channel is given by:

$$C_{\text{CCMC}}^{\text{Nak}} = \mathrm{E}\left\{\log_2(1+r\gamma_1)\right\}, \quad (8)$$

where the received SNR γ_1 of the Gaussian channel is weighted by the Nakgami-m channel's envelope r, which obeys the PDF of Eq. (5). The resultant capacity has to be averaged by either summation or integration over the specific range of SNRs encountered. The CCMC capacity, as the terminology suggested, assumes a continuous-amplitude optimally-distributed signal input, where the capacity is only limited by the transmit energy and by the bandwidth [17], [19]. However, the DCMC capacity considers both the effects of having discrete inputs as well as the specifics non-Gaussian distributed transmit signal of the digital modulation scheme [17]. Hence, it is more appropriate for our DSCM design. The DCMC capacity can be expressed as follows [20]:

$$C_{\text{DCMC}}^{\text{Nak}} = \max_{p(\mathbf{x}_1 \cdots \mathbf{x}_M)} \sum_{m=1}^{M} \int_{-\infty}^{\infty} \cdots \int_{-\infty}^{\infty} p(\mathbf{y} \mid \mathbf{x}_m) p(\mathbf{x}_m) \cdot \log_2 \left[\frac{p(\mathbf{y} \mid \mathbf{x}_m)}{p(\mathbf{y})}\right] d\mathbf{y} \quad \text{[bit/sym]} \quad (9)$$

where again, the channel's input $\mathbf{x}_m = \{x_m^1, x_m^2, \cdots, x_2^N\}$ is constituted by M-ary symbols with N-dimensional size and $\mathbf{y} = \{y^1, y^2, \cdots, y^N\}$ is the received signal with N-dimensional size. The conditional probability $p(\mathbf{y} \mid \mathbf{x}_m)$ can be determined using the PDF of the Nakagmi-m channel in Eq. (5). Furthermore, Eq. (9) can be be simplified to [17], [19]:

$$C_{\text{DCMC}} = \log_2(M) - \frac{1}{M}\sum_{m=1}^{M} \mathrm{E}\left[\log_2 \sum_{i=1}^{M} \exp(\Psi_i^m)\right] \quad \text{[bit/sym]}, \quad (10)$$

where we have:

$$\Psi_i^m = \frac{-|\mathbf{y} - \mathbf{h} \cdot \mathbf{x}_m + \mathbf{n}|^2 + |\mathbf{n}|^2}{N_0}. \quad (11)$$

The DCMC capacity curves of our four different modulation modes namely of, BPSK, QPSK, 8PSK and 16QAM, associated with different Nakagami-m fading parameters are depicted in Fig. 3. As m increases, the achievable capacity of the Nakagami-m channel increase. For example, when we consider the case of 16QAM in Fig. 3, as the fading parameter increases from $m = 1$ to $m = 4$, the capacity approaches that of the AWGN channel. It is also shown in Fig. 3 that increasing the fading parameter from $m = 1$ to $m = 2$ significantly improves the achievable capacity. However, the improvements will become more marginal for $m > 3$.

m	p_e	ρ	η_{SW}	$\eta_{10^{-5}}$	SW gap	Γ_{lim}	Γ	SW/S gap
1	0.1	0.80	0.469	0.55	0.081	-2.5	-2.2	0.3
	0.2	0.60	0.722	0.8	0.078	0	0.9	0.9
	0.3	0.40	0.881	0.99	0.109	3.5	5.2	1.7
2	0.1	0.80	0.469	0.52	0.051	-3.5	-3.1	0.4
	0.2	0.60	0.722	0.77	0.048	-1.5	-0.5	1.0
	0.3	0.40	0.881	0.94	0.059	1.15	3.0	1.85
6	0.1	0.80	0.469	0.49	0.021	-3.9	-3.3	0.6
	0.2	0.60	0.722	0.74	0.018	-2.0	-1.2	0.8
	0.3	0.40	0.881	0.91	0.03	0.0	1.7	1.7

TABLE I: System performance of the DSCM-QPSK/BPSK for SW coding over Nakagami-m fading channel, where the rates are recorded at BER $= 10^{-5}$.

[4]Further details of the decoding process can be found in [13].

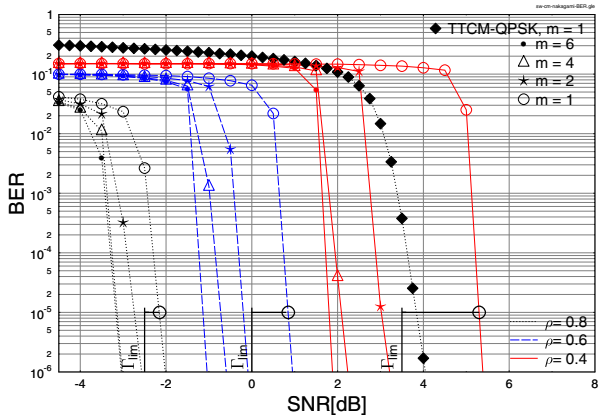

Fig. 4: BER versus SNR performance comparison of DSCM-QPSK/BPSK scheme when transmitting over Nakagami-m fading channels with different $m = \{1.0, 2.0, 4.0, 6.0\}$ where the correlation parameters are $\rho = \{0.4, 0.6, 0.8, 0.86\}$. The number of decoding iterations is $I = 8$.

To design our adaptive scheme, we commence by characterising the BER performance of the lowest throughput DSCM scheme, where the QPSK/BPSK mode is employed. Fig. 4 illustrates the BER performance of our scheme for a range of correlations $\rho = \{0.8, 0.6, 0.4\}$ and for fading parameters of $m = \{1.0, 2.0, 4.0, 6.0\}$, respectively. Note that the SNR is given by $\text{SNR(dB)} = E_b/N_0\text{(dB)} + 10\log_{10}(R_1)$. Here we employ a half-rate TTCM code associated with $N_S = 12\,000$ symbols in each of the encoding blocks, and with $I = 8$ decoding iterations. As shown in Fig. 4, all proposed DSCM schemes (except for the scheme having a low correlation of $\rho = 0.4$ with a fading parameter of $m = 1$) outperform the classical TTCM-aided QPSK benchmark scheme, which is labelled by filled diamonds, while dispensing with side information. To elaborate further, at a BER of 10^{-5} and $\rho = 0.8$, our distributed scheme is capable of attaining coding gains of 6.2 dB, 6.7 dB, 7.6 dB and 7.6 dB for $m = 1$, $m = 2$, $m = 4$ and $m = 6$, respectively. The BER performances of the proposed system associated with $\rho = 0.6$ and $\rho = 0.4$ exhibits a similar trend, as shown in Fig. 4. However, as expected, for a low correlation value the proposed scheme has an SNR loss of 1.3 dB, namely when we have $\rho = 0.4$ and $m = 1$. The impact of different m values on the attainable BER performance can be also seen in Fig. 4, where as illustrated in the DCMC curves of Fig 3, when m decreases, the BER performance will be degraded, since the fading becomes more severe.

In order to approach the SW/S bound, we first have to quantify the minimum required SNR Γ_{lim}. This minimum SNR can be inferred from Fig 3, for example when aiming for a target throughput of $\eta_{SW} = 0.469$ BPS for the DSCM-QPSK/BPSK scheme associated with $m = 2$, the DCMC curve indicates a minimum SNR of $\Gamma_{\text{lim}} = -2.5$ dB, as depicted in Fig. 3. Note that Γ_{lim} for the fading parameter $m = 1$ is shown with the aid of the vertical lines seen in Fig. 4, where it may be observed that at BER$= 10^{-5}$ and $m = 1$ the minimum distance with respect to the SW/S bound increases, as the correlation ρ between the sources reduces. Furthermore, both the SW theoretical bound and the achievable rates obtained for the DSCM-QPSK/BPSK schemes considered are presented in Fig. 5. These rates correspond to a BER level of 10^{-5} and on average the system's throughput is only 0.088 bits away from the bound. The DSCM-QPSK/BPSK performance against the SW(bits) bound as well as against the SW/S(dB) limit are tabulated in Table. I for different Nakagami-m fading values.

IV. Simulation Results

In practical DSC designs, adaptive coded modulation schemes are required for counteracting both the near-instantaneous time-varying nature of the wireless channel as well as the time-variant

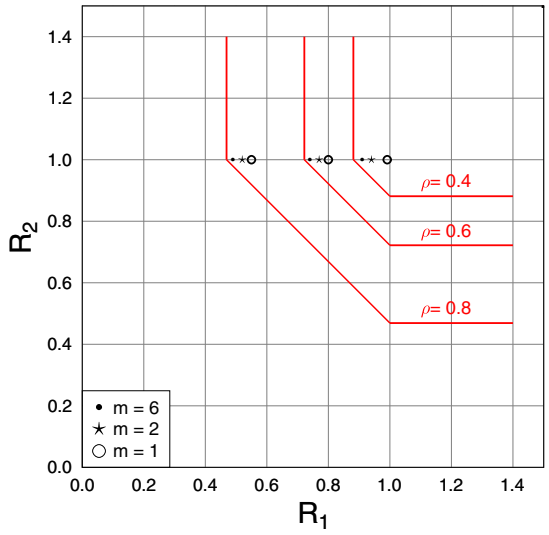

Fig. 5: Theoretical SW bound as well the rates (R_1, R_2) achieved by the proposed DSCM-QPSK/BPSK scheme for different p_e values, where Γ denotes the SNR required for achieving a BER = 10^{-5}.

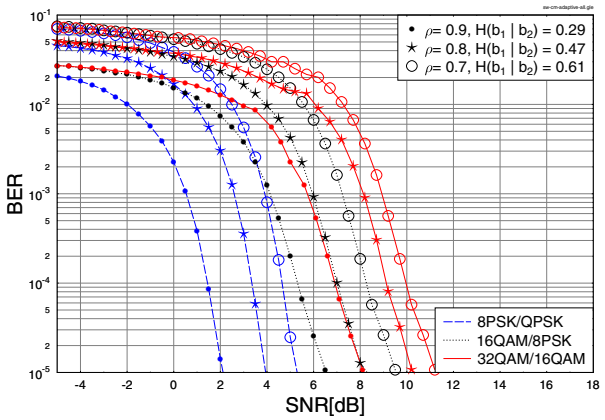

Fig. 6: BER versus SNR performance comparison between different transmission modes for correlation parameters of $\rho = \{0.7, 0.8, 0.9\}$ when transmitting over Nakagami-m fading channels with $m = 4$.

correlations between the two sources. In our simulations, we invoke the novel near-instantaneously adaptive scheme of [13] in which different modulation modes are chosen according to the particular near-instantaneous SNR of $\gamma_r = 10\log_{10}\left(|h|^2/N_0\right)$ [dB]. Before conceiving our adaptive scheme, we shall first examine the BER performance of the higher-order modulation modes. The performance of DSCM schemes employing the "8PSK/QPSK", "16QAM/8PSK" and "32QAM/16QAM" modes, for $\rho = \{0.7, 0.8, 0.9\}$ is shown Fig. 6, when communicating over Nakagami-m fading channels associated with $m = 4$. Again, a block length of $N_S = 12\,000$ symbols is used for all the modulation modes invoked for a total of 10 000 blocks, while the number of decoding iterations is $I = 8$. The performance of the higher-order modulation schemes simulated in Fig. 6 exhibits no error floor hence suggesting that the A-DSCM is readily applicable to SW coding in wireless applications. Similar to the QPSK/BPSK case, which was considered in Section. II, the least significant bit of each TTCM coded symbol will be punctured, hence resulting in puncturing rates of $R_p = \{3/2, 4/3, 5/4\}$ for "8PSK/QPSK", "16QAM/8PSK" and "32QAM/16QAM", respectively. It can be observed in Fig. 6 that the "8PSK/QPSK" scheme outperforms its counterparts using higher order modulation schemes. More explicitly, at a BER level of 10^{-5} and $\rho = 0.9$, the

"8PSK/QPSK" scheme has an SNR gain of 4.2 dB and of 6 dB in comparison to the "16QAM/8PSK" and "32QAM/16QAM" schemes, respectively. However, the "32QAM/16QAM" scheme associated with $\rho = 0.9$ outperforms the "16QAM/8PSK" associated with the lower correlation parameter of $\rho = 0.7$. Thus the effect of correlation becomes more dominant in higher-order modulation modes.

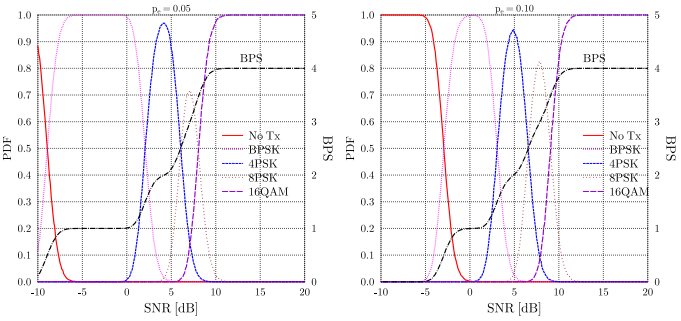

(a) $\rho = 0.90$. (b) $\rho = 0.80$

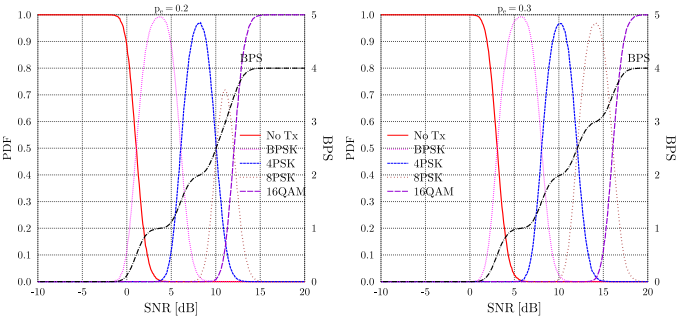

(c) $\rho = 0.60$ (d) $\rho = 0.40$

Fig. 7: PDF(left axis) and BPS(right axis) of all DSCM modes versus the SNR corresponding to correlation parameters of $\rho = \{0.9, 0.8, 0.6, 0.4\}$, when communicating over Nakagami-m fading channels with $m = 4$.

Fig. 7 portrays the Probability Density Function (PDF) along with the corresponding Bit Per Symbol (BPS) throughput of all of the DSCM modes against the received SNR for different crossover probabilities of $p_e = \{0.05, 0.10, 0.20, 0.30\}$, respectively. For each received block both the crossover probability as well as the near-instantaneous SNR γ_r are estimated and compared to a look-up table. Then, if γ_r is higher than the threshold γ_{th}, then the decoding will proceed. Otherwise, the BER of the received block will be estimated if BER $> 10^{-5}$, and a feedback acknowledgement flag will be transmitted to the transmitter, requesting a reduction of the transmission throughput[5]. Hence, our adaptive scheme maintains BER $< 10^{-5}$. Fig. 7 reveals that, as the SNR increases, the higher-order DSCM modes are most likely to be activated, than the lower-order ones. Thus, the aggregate BPS throughput increases smoothly along with the SNR. It may also be observed from the figure that in the presence of a high correlation between the two sources, such as $\rho = 0.9$, the 'no transmission' mode has effectively 'disappeared'. However, for low correlations the scheme requires a higher SNR for achieving a non-zero throughput. The adaptive procedure operates as follows: first the BER of each received block is estimated. Then provided that we have BER $< 10^{-5}$, a higher-order modulation mode will be requested for the next block.

V. Conclusions

In this paper, we investigated the performance of a reduced-complexity adaptive DSCM scheme communicating over a variety of realistic Nakagami-m fading channels. The DCMC capacity of the Nakgami-m channel was derived in order to estimate the SW/S bound. Moreover, our proposed scheme exhibited a robust performance for a wide range of source correlations. At a BER level of 10^{-5} associated with $p_e = 0.1$ and $m = 2$, the proposed scheme operates within 0.4 dB from the theoretical SW/S bound, where it is only 0.052 bits away from the maximum achievable SW compression bound. Finally, our scheme shows the best result reported in the literature for similar systems, whilst considering a wide range of realistic fading channel models.

[5]The follow chart in [13] explains the process in further details.

References

[1] Z. Xiong, A. Liveris, and S. Cheng, "Distributed source coding for sensor networks," *IEEE Signal Process. Mag.*, vol. 21, no. 5, pp. 80–94, Sept. 2004.

[2] V. S. Qian Xu and Z. Xiong, "Distributed joint source-channel coding of video using raptor codes," *IEEE J. Sel. Areas Commun.*, vol. 25, no. 4, pp. 851–861, 2007.

[3] S. Wang, L. Cui, S. Cheng, L. Stankovic, and V. Stankovic, "Onboard low-complexity compression of solar stereo images," *IEEE Trans. Image Process.*, vol. 21, no. 6, pp. 3114–3118, 2012.

[4] D. Slepian and J. K. Wolf, "Noiseless coding of correlated information sources," *IEEE Trans. Inform. Theory*, vol. 19, no. 8, pp. 471–480, Jul 1973.

[5] J. Garcia-Frias and Z. Xiong, "Distributed source and joint source-channel coding: from theory to practice," in *Proc. IEEE Int. Conf. on Acoustics, Speech, and Signal (ICASSP).*, vol. 5, March 2005, pp. 1093–1096.

[6] A. Aaron, and B. Girod, "Compression with side information using turbo codes," in *Proc. of the Data Compression Conf. (DCC)*, 2002, pp. 252–261.

[7] D. Varodayan, A. Aaron, and B. Girod, "Rate-adaptive codes for distributed source coding," *Elsevier Signal Process.*, vol. 86, no. 11, pp. 3123–3130, Nov. 2006.

[8] A. Liveris, Z. Xiong, and C. Georghiades, "Compression of binary sources with side information at the decoder using LDPC codes," *IEEE Commun. Lett.*, vol. 6, no. 10, pp. 440–442, Oct. 2002.

[9] X. Lv, R. Liu, and R. Wang, "A novel rate-adaptive distributed source coding scheme using polar codes," *IEEE Commun. Lett.*, vol. 17, no. 1, pp. 143–146, 2013.

[10] J. Garcia-Frias and Y. Zhao., "Near-Shannon/Slepian-Wolf performance for unknown correlated sources over AWGN channels," *IEEE Trans. Commun.*, vol. 53, no. 4, pp. 555–559, April 2005.

[11] Y. Zhao, W. Zhong, and J. Garcia-Frias, "Transmission of correlated senders over a Rayleigh fading multiple access channel," *Elsevier Signal Process.*, vol. 86, no. 11, pp. 3150–3159, April 2006.

[12] K. Anwar and T. Matsumoto, "Iterative spatial demapping for two correlated sources with power control over fading MAC," *Proc. IEEE Vehicular Technology Conf. (VTC) Spring*, pp. 1–7, May 2012.

[13] A. J. Aljohani, S. X. Ng and L. Hanzo, "TTCM-aided rate-adaptive distributed source coding for Rayleigh fading channels," *IEEE Trans. Veh. Technol.*, vol. PP, no. 99, pp. 1–1, 2014.

[14] P. Robertson and T. Wörz, "Bandwidth-efficient turbo trellis-coded modulation using punctured component codes," *IEEE J. Sel. Areas Commun.*, vol. 16, no. 2, pp. 206–218, Feb. 1998.

[15] M. Nakagami, *The M-distribution - A General Formula of Intensity Distribution of Rapid Fading*, W. C. Hoffman, Ed. Pergamon Press, 1960.

[16] L. Hanzo and T. H. Liew, B. L. Yeap and S. X. Ng, *Turbo Coding, Turbo Equalisation and Space-Time Coding: EXIT-Chart Aided Near-Capacity Designs for Wireless Channels*. John Wiley & Sons, 2010.

[17] S. X. Ng and L. Hanzo, "On the MIMO channel capacity of multi-dimensional signal sets," *IEEE Trans. Veh. Technol.*, vol. 55, pp. 528–536, March 2006.

[18] J. Del Ser, P. Crespo, and A. Munoz, "Joint source-channel decoding of correlated sources over ISI channels," in *IEEE Vehicular Technology Conf. (VTC) Spring.*, vol. 1, June 2005, pp. 625–629.

[19] J. Proakis, *Digital Communications*, 4th ed. New York, USA: McGraw-Hill, 2000.

[20] M. Campanella and G. Mamola, "On the channel capacity for constant envelope signals with effective bandwidth constraint," *IEEE Trans. Commun.*, vol. 38, no. 8, pp. 1164–1172, August 1990.